A plausible mechanism for longitudinal lock-in of cortical microtubule array after light-induced reorientation

Marco Saltini[a] and Bela M. Mulder
AMOLF, Science Park 104, 1098XG Amsterdam, The Netherlands

The light-induced reorientation of the cortical microtubule array in dark-grown *A. thaliana* hypocotyl cells is a striking example of the dynamical plasticity of the microtubule cytoskeleton. A consensus model, based on *katanin*-mediated severing at microtubule crossovers, has been developed that successfully describes the onset of the observed switch between a transverse and longitudinal array orientation. However, we currently lack an understanding of of why the newly populated longitudinal array direction remains stable for longer times, when the initial trigger for the reorientation has died out, and re-equilibration effects would tend to drive the system back to a mixed orientation state. Using both simulations and analytical calculations, we show that the assumption of a small orientation-dependent shift in microtubule dynamics is sufficient to explain the long term lock-in of the longitudinal array orientation. Furthermore, we show that the natural alternative hypothesis that there is a selective advantage in severing longitudinal microtubules, is neither necessary nor sufficient to achieve cortical array reorientation, but is able to accelerate this process significantly.

[a] Current affiliation: Uppsala University, Department of Ecology and Genetics, Animal Ecology, Norbyvägen 18D, 752 36 Uppsala, Sweden.

I. INTRODUCTION

The cortical microtubule array (hereafter CA) is a highly ordered structure occurring in cells of higher plants, which plays a key role in the growth-driven morphogenesis of cells and, therefore, also of the organism as a whole. It is known that the function of the CA is intimately linked to its spatial organization which, in turn, is linked to its dynamic properties [1]. In contrast to animal cells, the CA is built and reorganized without benefit of a microtubule organizing centre (centrosome). Instead, new microtubules in the CA are generated in two distinct ways: from nucleation templates - i.e., γ-tubulin complexes, mostly located on the lattice of already existing microtubules [2, 3], or from severing events of already-existing microtubules. The latter mode of generation of new microtubules is mediated by the severing protein *katanin* that localizes at microtubule crossovers and preferentially severs the newer one, i.e., the overlying one [4]. It plays a crucial role in the reorientation of the cortical array as a response to blue light. Typically, the direction of the cortical microtubule array of growing plant cells is transverse to the long axis of the cell. However, upon exposure to blue light, in dark-grown hypocotyl cells of *Arabidopsis thaliana*, the initially transverse array undergoes a striking reorientation to a direction longitudinal to the long axis of the cell. Since the initial array is transverse to the long axis of the cell, newer microtubules at crossovers are most likely longitudinal and, hence, the occurrence of multiple severing events quickly generates a new exponentially growing population of longitudinal microtubules [4].

Experimental and computational studies have identified the crucial role of the stability of the dynamic microtubule ends in enabling CA reorientation [5, 6]. Furthermore, a recent theoretical study has shown that the combination of preferential severing and a high probability of stabilization-after-severing for the newly-created microtubule plus-ends is a necessary ingredient for the reorientation process to start [7]. However, these studies focused on the first phase of the reorientation process, when the initial transverse array can still be seen as a constant background and free tubulin to build new microtubules is likely available in abundance. While these assumptions are realistic at the start of the reorientation process, at a later phase the amount of free tubulin is bound to become scarce as the number of growing microtubules increases. As transverse microtubules are also dynamic, this scarcity of tubulin would imply their gradual depolymerization, as they are outcompeted by the large population of growing longitudinal microtubules. This in turn, however, decreases the opportunity to create new crossovers and, therefore, to create new longitudinal microtubules from severing events. This suggests that while the initial asymmetry in the number of preferential severing of microtubules in the longitudinal direction is a sufficient ingredient to yield an initial asymmetry between the two populations of differently oriented microtubules, over time this bias is expected to fade. New transverse microtubules will start to be nucleated, and their crossovers with preexisting longitudinal microtubules can now serve to generate more transverse ones, through the same severing mechanism. In fact, all things being equal, one would expect the system to evolve to a novel steady state with an equal number of transverse and longitudinal microtubules. This clearly contrasts with the experimental findings of an ultimately stable longitudinal array, and raises the question of the mechanism by which this switch in orientations can be maintained.

Here, we explore the hypothesis that the ultimate asymmetry between differently oriented microtubules could be a consequence of small differences in their dynamic behaviour. The idea that the dynamics of microtubules can be influenced by cell geometry has received a lot of attention since the seminal work of Hamant et al. [8] (for a review see [9]) which provided the first evidence that microtubule would in fact prefer to align in the direction of maximal stress in the cell wall. In the most common cylindrical plant cell geometry this direction of maximal stress follows the direction of strongest curvature, which thus provides a possible explanation for the ubiquitous transversality of the CA in this cell geometry. Although the severing protein katanin is implicated in mediating the interaction between wall stress and microtubule stabilisation [10], the precise mechanism by which this occurred has not been elucidated to date. Computational models of cortical microtubule dynamics on closed surfaces with different geometries have also shown that slight directional cues, caused, e.g., by catastrophes induced at sharp cell edges or relative stabilization on specific cell faces, are sufficient to select a single preferential direction of ordering of the CA as a whole [11, 12]. On the basis of these considerations, we posit that a mechanism by which microtubule dynamics is sensitive to orientation with respect to a cell axis is possible, and that such a bias can impact the global organisation of the CA. Specifically, we will assume that microtubules in the longitudinal direction will grow slightly faster than ones in the transverse direction, but, as we show, an analogous decrease of catastrophe rate in the longitudinal direction will serve the same purpose.

We implement our hypothesis in a stylized stochastic model of dynamic microtubules that can only occur in two distinct orientations - i.e., transverse and longitudinal. These two populations of microtubules compete for the same pool of available tubulin dimers as their building material. Besides the indirect interaction through the available tubulin pool, the two populations of microtubules directly interact through severing events at crossovers. Both simulations and additional analytical calculations show that the small difference in the dynamic parameters between the two populations can explain the experimentally observed lock-in of the CA to the longitudinal direction after reorientation from an initially transverse state. We also test an alternative hypothesis that the preferential severing of longitudinal microtubules is specifically required for the reorientation to occur. While we show that the latter mechanism is neither

a necessary nor a sufficient ingredient for the reorientation to occur, we do find that it can significantly increase the speed of the reorientation.

II. METHODS

To test our hypothesis that the full, maintained reorientation of the CA (see Figure 1A) is caused by a small asymmetry in the dynamics of differently oriented microtubules, we introduce a stochastic model for microtubules undergoing dynamic instability. We focus on the generation of new microtubules through nucleation and severing. A full mathematical description of the system of differential equations controlling the dynamics of individual microtubules and the steady-state solution for microtubule length distribution can be found in the Supplementary Information VI A.

The model

The model, based on the Dogterom-Leibler model for microtubule dynamics [13] consists of two populations of microtubules undergoing dynamic instability: longitudinal ($M_{\parallel}$) and transverse ($M_{\perp}$).

Tubulin redistribution

The two populations compete for a finite tubulin pool, i.e., they can access a finite amount of building material for growing and being nucleated. Let L_{tot} be the total amount of tubulin in the system. Then, L_{tot} is divided in three different populations: free tubulin pool L_f, tubulin used by longitudinal microtubules $L_{\parallel}$, and tubulin used by transverse microtubules $L_{\perp}$, such that

$$L_{tot} = L_f + L_{\parallel} + L_{\perp}, \tag{1}$$

see Figure 1B. The finiteness of the tubulin pool has practical consequences on the dynamics of microtubules. In particular, the abundance of free tubulin is positively correlated to both the nucleation rate and the growing speed of microtubules.

Nucleation of new microtubules

Experiments [14] have identified a Hill relation between the nucleation rate of new microtubules and the abundance of free tubulin, i.e.,

$$R_n\left(L_f\right) = r_n \frac{L_f^a}{L_f^a + L_v^a}, \tag{2}$$

where $a \simeq 6$, L_v is a constant length-scale expression of finiteness of the pool and diffusion of the free tubulin, and r_n is the nucleation rate of new microtubules in case of unbounded availability of tubulin.

Consistently with *in vivo* observations [15], we assume that microtubules are mainly - but not exclusively, created by microtubule-based nucleation. In particular, we divide the nucleation of new microtubules in two distinct nucleation types: microtubule-based nucleation and nucleation from a dispersed site, with nucleation rates, respectively,

$$R_{n,b} = R_n\left(L_f\right) \frac{L_{\parallel} + L_{\perp}}{L_{\parallel} + L_{\perp} + L_*}, \tag{3}$$

and

$$R_{n,u} = R_n\left(L_f\right) \frac{L_*}{L_{\parallel} + L_{\perp} + L_*}. \tag{4}$$

L_* is the *propensity length for dispersed nucleation*, i.e., a constant that controls the fraction of nucleation events that occur from dispersed sites in the cytosol rather than from the lattice of already existing microtubules.

In the cortical microtubule array, a newly-generated microtubule through microtubule-based nucleation is nucleated preferentially parallel or with an angle of about 40° with respect to the growth direction of the mother microtubule

[16, 17]. This suggests the existence of a nucleation mechanism that roughly maintains the orientation of the microtubule array. As here we only consider two possible directions for microtubules, we assume that new microtubules generated through microtubule-based nucleation have a strong bias towards growing in the same direction as the mother microtubule. We include this mechanism in our model by introducing the probability $z > 1/2$ for a new microtubule to be nucleated parallel to the mother microtubule, and consequently $1 - z$ to be nucleated orthogonal to it. Then, the microtubule-based nucleation rates for new longitudinal and transverse microtubules are, respectively,

$$R^{\parallel}_{n,b} = R_n\left(L_f\right)\frac{zL_{\parallel} + (1-z)\,L_{\perp}}{L_{\parallel} + L_{\perp} + L_*}, \tag{5}$$

and

$$R^{\perp}_{n,b} = R_n\left(L_f\right)\frac{(1-z)\,L_{\parallel} + zL_{\perp}}{L_{\parallel} + L_{\perp} + L_*}. \tag{6}$$

We reasonably assume that the medium is isotropic as regards the dispersed nucleation of new microtubules. Hence, the rates for dispersed nucleation are

$$R^{\parallel}_{n,u} = R^{\perp}_{n,u} = R_n\left(L_f\right)\frac{\frac{1}{2}L_*}{L_{\parallel} + L_{\perp} + L_*}. \tag{7}$$

It follows that the overall nucleation rates for the two populations are $R^{\parallel}_n = R^{\parallel}_{n,u} + R^{\parallel}_{n,b}$ and $R^{\perp}_n = R^{\perp}_{n,u} + R^{\perp}_{n,b}$, see Figure 1C.

Dynamics of individual microtubules

All microtubules are nucleated in the growing state, with growing speed V^+. Experiments have revealed that the growing speed is seemingly linear in the amount of free tubulin [14]. Here, however, to be consistent with Eq. (2), and to include saturation in the growing speed of microtubules, we assume the growing speed to be

$$V^+\left(L_f\right) = v^+\frac{L_f}{L_f + L_v}. \tag{8}$$

It is important to underline that our choice and the experimental observations could be only apparently discrepant. Indeed the limit of long L_v of Eq. (8) would imply a linear relation between growing speed and abundance of free tubulin, resulting in the agreement between our model assumption and the experimental observations. Growing microtubules can switch from the growing to the shrinking state with constant catastrophe rate r_c. Microtubules in the shrinking state shrink with constant speed v^-, and they can switch from the shrinking to the growing state with rescue rate r_r.

When differently oriented microtubule cross each others they create a crossover, where a severing event can take place. In particular, the occurrence or not of a severing event is partly influenced by the number of crossovers a microtubule has created and, consequently, to its length, and partly by its relative position to the crossing microtubule. Indeed, experiments have shown a preferential severing for newer microtubules, i.e., microtubules who lay on top of already existing ones [4]. Since our model consists of two populations of non-interacting microtubules, to model the creation of crossovers and the occurrence of severing events we introduce an effective severing rate for an individual microtubule proportional to the product between its length and the total amount of tubulin polarized in its opposite direction. Furthermore, to be consistent with the experimental observations that new microtubules are, in general, longitudinally oriented, we introduce a preferential severing for the latter by assuming a probability $q > \frac{1}{2}$ of severing a longitudinal microtubule given that a severing event has occurred. Then, if r_s is the intrinsic severing rate at a crossover, the overall severing rates for longitudinal and transverse microtubules of length l are, respectively,

$$R_{s,\parallel}\left(l\right) = qr_s l L_{\perp}, \tag{9}$$

and

$$R_{s,\perp}\left(l\right) = (1-q)\,r_s l L_{\parallel}. \tag{10}$$

Once a microtubule is severed, the newly-created plus end of the lagging microtubule enters either the growing state with probability of stabilization-after-severing p^+, or the shrinking state with probability $1 - p^+$, while no changes are applied to the state of the plus end of the leading microtubule. Experimental and theoretical works have shown that a relatively high probability of stabilization-after-severing ($p^+ \simeq 0.15$) is required in order to commence the reorientation process [6, 7]. Finally, the newly-created minus end of the leading microtubule remains stable, without undergoing dynamic instability, see Figure 1D.

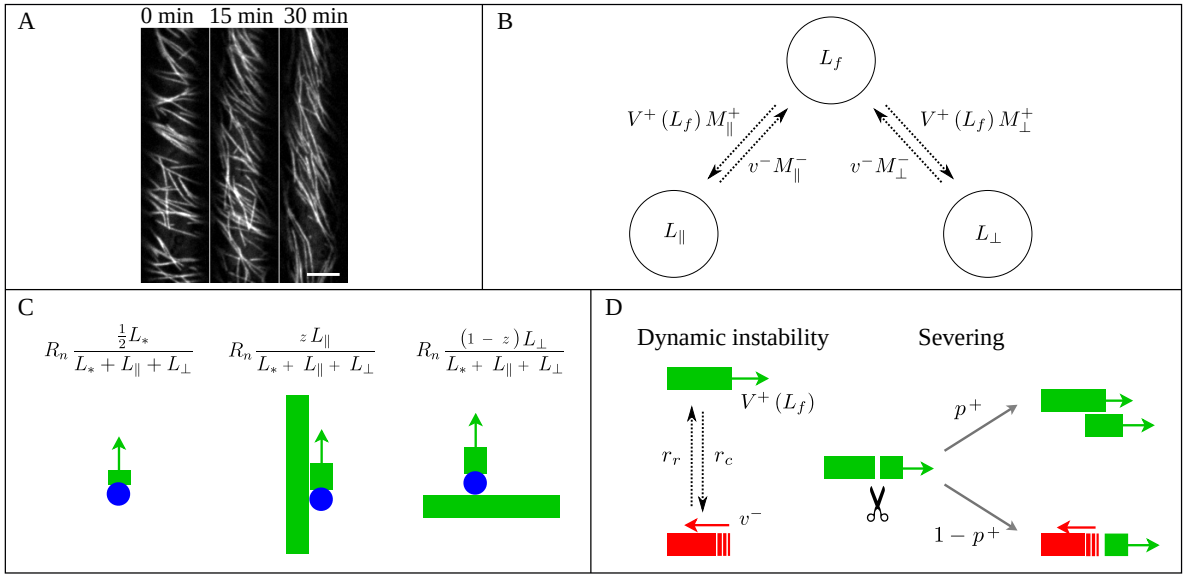

Figure 1. (A) Microtubule reorientation of dark-grown hypocotyl cells at 0, 15, and 30 min after induction of reorientation by blue light. Scale bar, 5 μm. (B) Overall dynamics of the two microtubule populations and tubulin redistribution in the system. Free tubulin is recruited by microtubules of the two dynamic populations with a speed proportional to the total number of growing microtubules, while it returns to the free pool with a speed proportional to the total number of shrinking microtubules. The label $\pm$ stands for growing/shrinking, respectively. (C) Nucleation rates for new longitudinal microtubules. From left to right, new microtubules can be nucleated through dispersed nucleation, microtubule-based nucleation parallel to the mother longitudinal microtubule, or microtubule-based nucleation orthogonal to the mother transverse microtubule. Blue circles represent the γ-tubulin complex. (D) Dynamics of an individual microtubule. Microtubules undergo dynamic instability and are severed with rate proportional to their length. Newly-created plus end after severing enters either the growing state with probability p^+, or the shrinking state with probability $1-p^+$.

Small increase in the growing speed of longitudinal microtubules

Previous works on the effect of cell geometry on microtubule dynamics have revealed that the mechanical stress induced by cell wall geometry can influence the alignment of cortical microtubules [8, 9]. Furthermore, computational works have shown that slight directional cues caused by, e.g., catastrophes or microtubule stabilization induced by surface geometry, can select a single preferential alignment of the CA [11, 12].

Plant cells can well be approximated by a cylinder. Thus, transverse microtubules undergo dynamic instability on a curved surface while longitudinal microtubules undergo dynamic instability on a roughly flat surface. Consequently, we propose that a mechanism by which microtubule dynamics can be influenced by their orientation with respect to the cell axis is plausible. Specifically, we hypothesize that longitudinal microtubules grow slightly faster than transverse microtubules, and that such a bias is a sufficient ingredient to obtained a maintained reorientation of the CA. Therefore, we set

$$v_\parallel^+ = \alpha v_\perp^+ \equiv \alpha v^+, \tag{11}$$

with $\alpha > 1$ and $\alpha \simeq 1$. No changes are applied to the other dynamic parameters of the model. Our choice of applying a difference only in the growing speed is motivated by a practical reason. Indeed, changing only the growing speed would make the model analytically tractable. Nevertheless, in the Result section we will show that applying the difference to the two growing speeds has the same effect on the steady-state properties of the system as applying the difference to the catastrophe rates, suggesting that the choice of the dynamic parameter to vary in order to obtain a maintained reorientation is arbitrary.

Polarization and transverse suppression

We refer to the initial number of transverse microtubules as $M_\perp^0$, and to the tubulin utilized by them as $L_\perp^0$. To evaluate the efficiency of the reorientation, we define the following order parameters:

Parameter	Description	Numerical value	Units
v^+	Growth speed	0.103	$\mu\mathrm{m\,s}^{-1}$
v^-	Shrinkage speed	0.225	$\mu\mathrm{m\,s}^{-1}$
r_c	Catastrophe rate	0.01	s^{-1}
r_r	Rescue rate	0.026	s^{-1}
r_s	Severing rate	$2 \cdot 10^{-7}$	$\mathrm{s}^{-1}\ \mu\mathrm{m}^{-2}$
r_n	Nucleation rate	0.3	s^{-1}
α	Speed bias	1.1	-
p^+	Stabilization-after-severing	Tuned	-
q	Sever probability (longitudinal microtubules)	Tuned	-
L_{tot}	Total amount of tubulin	$4 \cdot 10^3$	μm
L_v	Crossover length	$8 \cdot 10^2$	μm
L_*	Propensity length for dispersed nucleation	10^2	μm
z	Probability of nucleation parallel to the parent	0.9	-

Table I. Reference values for the parameters of the model. Numerical values for the dynamic parameters and the amount of tubulin has been chosen consistently with experimental measurements [6, 14].

- *number* and *length polarization*, respectively,

$$\mathcal{P}_M = \frac{M_\parallel - M_\perp}{M_\parallel + M_\perp}, \qquad \mathcal{P}_L = \frac{L_\parallel - L_\perp}{L_\parallel + L_\perp},$$

  as order parameters for the difference between the two populations,

- *number* and *length transverse suppression*, respectively,

$$\mathcal{R}_M = \frac{M_\perp^0 - M_\perp}{M_\perp^0 + M_\perp}, \qquad \mathcal{R}_L = \frac{L_\perp^0 - L_\perp}{L_\perp^0 + L_\perp},$$

  as order parameters that estimate how much of the original transverse array is still present at the end of the process.

Ideally, to consider the reorientation efficient, we require that all four order parameters are close to 1, i.e., most of microtubules and the used tubulin are polarized in the longitudinal direction, and that the time scale for the array to reorient is comparable to the experimentally observed one [4, 6].

III. RESULTS

A. Computational approach

We run stochastic simulations of our model to asses weather the difference in growing speed between the two different populations is sufficient to achieve a full, maintained reorientation of the array. Simulations initially consist of a transverse array at the equilibrium, see Supplementary Information VI B. Then, at time $t = 0$, we allow the nucleation of longitudinal microtubules both through microtubule-based nucleation and dispersed nucleation. We let the simulations run until the system reaches a steady-state and, then, we measure number and length polarization and suppression, and the required time to obtain a full reorientation of the CA. We perform a sensitivity analysis in the (q, p^+) plane by separately tuning them from 0 to 1. We average the results over $N = 10^3$ stochastic simulation *per* (q, p^+) couple. Parameters and relative numerical values used in the simulations are listed in Table I.

Figure 2ABCD shows the polarization and the transverse suppression for both microtubule number and length. Although the figure shows that a more efficient and fast reorientation requires high values of both q and p^+, we can still observe a good degree of reorientation for p^+ comprises between 0 and 0.25, i.e., in the biologically relevant range of values for the probability of stabilization-after-severing. In particular, the redistribution of tubulin seems to be very efficient in that range of values, see Figure 2BD. It is also interesting to notice that in such an area, polarization and suppression seem to be not strongly dependent on q. This suggests that, even though the preferential severing plays an important role in the amplification phase of the reorientation to boost the creation of longitudinal microtubules, in presence of biased speed it is not strictly necessary to maintain the new longitudinal array.

Figure 3 shows the time behaviour of the number and the total length of microtubules belonging to the different populations. The combination of preferential severing and biased speed has a double effect: it makes the reorientation

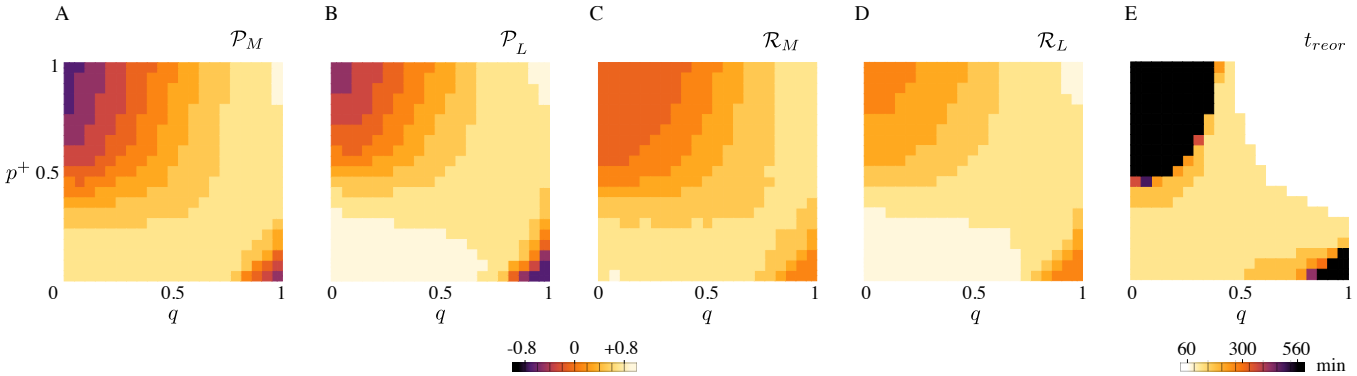

Figure 2. (A) Microtubule number polarization, (B) microtubule length polarization, (C) transverse number suppression, (D) transverse length suppression, (E) and transverse-to-longitudinal reorientation time as functions of q and p^+. Lighter colors correspond to a more efficient reorientation. (A, B, C, D) The range of values for polarization and suppression runs from -1 to $+1$. (E) Black areas in the (q, p^+) plane correspond both to reorientation processes that required more than 540 minutes, or non-occurred reorientation. Results are averaged over $N = 10^3$ simulations.

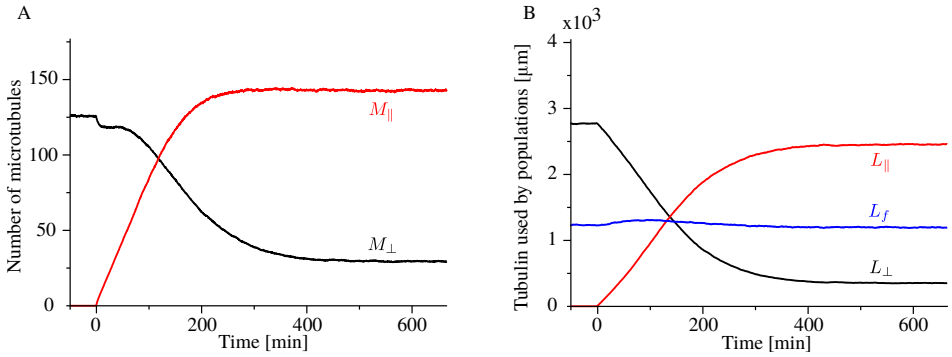

Figure 3. Time evolution of (A) longitudinal (red) and transverse (black) microtubules, and (B) tubulin used by the longitudinal population (red), the transverse population (black), and the free tubulin (blue), for $q = 0.75$, $p^+ = 0.15$.

efficient by increasing the number of longitudinal microtubules at the steady-state and suppressing the transverse, and it boosts the speed at which the reorientation occurs. Moreover, Figure 3B also shows that there is no appreciable difference between the amount of free tubulin at the beginning and at the end of the process. This means that the building material used by the longitudinal array comes from the initial transverse array rather than from the pool of free tubulin.

We also tested the alternative hypothesis that the factors that promote the commencement of the reorientation process, namely, high probability of stabilization-after-severing and preferential severing for longitudinal microtubules [6, 7], could be sufficient to explain the experimentally observed maintained reorientation. Our simulations showed that, although the two ingredients are indeed necessary to quickly start the reorientation process and reach a steady-state, they cannot explain how the full reorientation is achieved and maintained (see Supplementary Information VI C).

B. Analytical approach

To further test our hypothesis that reorientation and maintenance of the array are caused by a biased recruitment of tubulin towards the longitudinal microtubules, we analytically study a simplified version of our model in which the two populations of microtubules compete for the tubulin pool without direct interaction between them, i.e., without possibility of severing events. Therefore we set $r_s = 0$. We make the further simplification of assuming complete depolymerization of microtubules just after catastrophe events, i.e.,

$$\frac{\langle l \rangle}{v^-} \ll \frac{1}{r_r}, \tag{12}$$

where $\langle l \rangle$ is the average length of microtubules. Finally, we assume that all microtubules are nucleated in the same direction of the mother microtubule, i.e., $z = 1$. To ease the notation, if not strictly necessary, we hereafter drop the direct dependency of V^+ and R_n on L_f. Under these assumptions we can rewrite the dynamic Eqs. (37-40) as

$$\frac{\partial}{\partial t} m_{\parallel}(t,l) = -\alpha V^+ \frac{\partial}{\partial l} m_{\parallel}(t,l) - r_c m_{\parallel}(t,l), \tag{13}$$

$$\frac{\partial}{\partial t} m_{\perp}(t,l) = -V^+ \frac{\partial}{\partial l} m_{\perp}(t,l) - r_c m_{\perp}(t,l), \tag{14}$$

with boundary conditions

$$\alpha V^+ m_{\parallel}(t,0) = R_n^{\parallel}, \tag{15}$$

$$V^+ m_{\perp}(t,0) = R_n^{\perp}. \tag{16}$$

Moment equations

We study the 0^{th} and the 1^{st} moment equations corresponding to Eqs. (13) and (14), i.e.

$$\frac{d}{dt} M_{\parallel}(t) = R_n^{\parallel} - r_c M_{\parallel}(t), \tag{17}$$

$$\frac{d}{dt} M_{\perp}(t) = R_n^{\perp} - r_c M_{\perp}(t), \tag{18}$$

$$\frac{d}{dt} L_{\parallel}(t) = \alpha V^+ M_{\parallel}(t) - r_c L_{\parallel}(t), \tag{19}$$

$$\frac{d}{dt} L_{\perp}(t) = V^+ M_{\perp}(t) - r_c L_{\perp}(t), \tag{20}$$

coupled with the conservation of total tubulin

$$\frac{d}{dt} L_f(t) = -\frac{d}{dt} \left[L_{\parallel}(t) + L_{\perp}(t) \right]. \tag{21}$$

Suppose that $\alpha = 1$. Then, because of the symmetry between longitudinal and transverse microtubules, when longitudinal microtubules start to be nucleated the overall nucleation rate of all microtubules, as well as their growth rates, remain the same as in the initial system with only the transverse array. Therefore we can safely assume that, in that specific case, $L_f = const$. Here, since α is slightly greater than 1, if we make the reasonable assumption that L_f is smooth in α, it follows that

$$\frac{d}{dt} \left[L_{\parallel}(t) + L_{\perp}(t) \right] \simeq 0. \tag{22}$$

This last equation means that all building material used by the newer longitudinal array comes from the already existing transverse one, in agreement with our computational findings, see Figure 3.

Steady-state solution

In order to find a way to control the polarization of the tubulin, and hence the reorientation mechanism, we study the steady-state version of the moment Eqs. (17-20). If we isolate $r_c M_{\parallel}$ and $r_c M_{\perp}$ from the four equations we obtain

$$R_n^{\parallel} = r_c M_{\parallel} = \frac{r_c^2}{\alpha V^+} L_{\parallel}, \tag{23}$$

and

$$R_n^{\perp} = r_c M_{\perp} = \frac{r_c^2}{V^+} L_{\perp}. \tag{24}$$

From Eq. (23) we can observe that multiplying v^+ by α for the longitudinal growing speed is equivalent to divide r_c by $\sqrt{\alpha}$.

If we define

$$\lambda_{\parallel/\perp} \equiv \frac{L_{\parallel/\perp}}{L_{tot} - L_f}, \tag{25}$$

$$\lambda_* \equiv \frac{L_*}{L_{tot} - L_f}, \tag{26}$$

and we divide Eq. (23) by (24), by making use of Eqs. (5), (6), and (7) we obtain the system

$$\begin{cases} \frac{\lambda_\perp}{\lambda_\parallel} = \frac{\frac{1}{2}\lambda_* + \lambda_\parallel}{\alpha\left(\frac{1}{2}\lambda_* + \lambda_\perp\right)}, \\ \\ \lambda_\parallel + \lambda_\perp = 1. \end{cases} \tag{27}$$

The system can be solved to find

$$\lambda_\parallel = \frac{(\alpha-1) - \frac{1}{2}\lambda_*(\alpha+1) + \sqrt{\left[(\alpha-1) + \frac{1}{2}\lambda_*(\alpha+1)\right]^2 - 2\lambda_*(\alpha-1)}}{2(\alpha-1)}, \tag{28}$$

$$\lambda_\perp = \frac{(\alpha-1) + \frac{1}{2}\lambda_*(\alpha+1) - \sqrt{\left[(\alpha-1) + \frac{1}{2}\lambda_*(\alpha+1)\right]^2 - 2\lambda_*(\alpha-1)}}{2(\alpha-1)}. \tag{29}$$

If we divide both sides of Eq. (29) by $(\alpha-1) + \frac{1}{2}\lambda_*(\alpha+1)$ and we expand the square root we obtain

$$\lambda_\perp \simeq \frac{1}{2} \frac{\lambda_*}{(\alpha-1) + \frac{1}{2}\lambda_*(\alpha+1)}. \tag{30}$$

Consequently

$$\lambda_\parallel \simeq 1 - \frac{1}{2} \frac{\lambda_*}{(\alpha-1) + \frac{1}{2}\lambda_*(\alpha+1)}. \tag{31}$$

By plugging Eqs. (30) and (31) into Eqs. (23) and (24), we obtain the number of microtubules in the longitudinal and in the transverse directions

$$M_\parallel = \frac{R_n}{r_c} \frac{1}{\lambda_* + 1} \left[\frac{1}{2}\lambda_* \left(1 - \frac{1}{(\alpha-1) + \frac{1}{2}\lambda_*(\alpha+1)} \right) + 1 \right], \tag{32}$$

$$M_\perp = \frac{R_n}{r_c} \frac{\frac{1}{2}\lambda_*}{\lambda_* + 1} \left(1 + \frac{1}{(\alpha-1) + \frac{1}{2}\lambda_*(\alpha+1)} \right). \tag{33}$$

Notice that, in the $\lambda_* \to 0$ limit - i.e., when nucleation is only microtubule-based, all tubulin is polarized in the longitudinal direction, and then we observe full reorientation of the array from the transverse to the longitudinal direction. Indeed $\lim_{\lambda_* \to 0} \lambda_\parallel = 1$, and $\lim_{\lambda_* \to 0} M_\parallel = \frac{R_n}{r_c}$. On the other hand, when $\lambda_* \to \infty$ - i.e., when nucleation is only dispersed,

$$\lim_{\lambda_* \to \infty} \lambda_\parallel = \frac{\alpha}{\alpha+1}, \tag{34}$$

$$\lim_{\lambda_* \to \infty} \lambda_\perp = \frac{1}{\alpha + 1}, \tag{35}$$

$$\lim_{\lambda_* \to \infty} M_\parallel = \lim_{\lambda_* \to \infty} M_\perp = \frac{1}{2} \frac{R_n}{r_c}, \tag{36}$$

meaning that, although in such a limit the isotropy of the dispersed nucleation imposes that the final number of microtubules of the two populations is the same, the $\alpha > 1$ bias in the growing speed still produces a slight tubulin polarization in the longitudinal direction, with the only consequence of producing slightly longer longitudinal microtubules than transverse, see Figure 4.

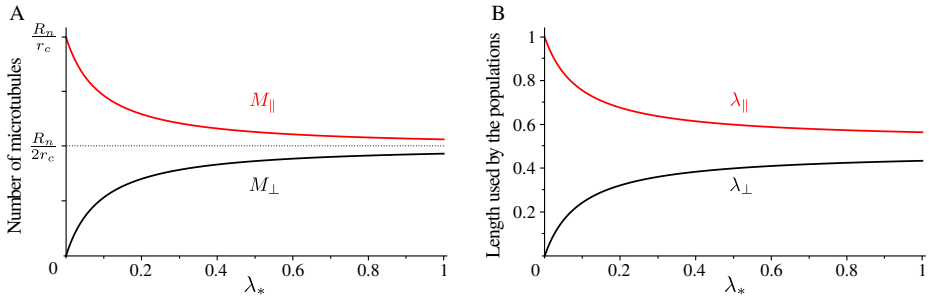

Figure 4. (A) Number of microtubules and (B) non-dimensional length used by microtubules populations as functions of the propensity length for dispersed nucleation, with $\alpha = 1.1$.

IV. DISCUSSION

We introduced a stochastic model for two populations of microtubules that compete for a shared pool of free tubulin - their building material, and interact with each others through severing events. Our model was based on the experimental observation that cortical microtubules of the cells of higher plants undergo a striking severing-driven reorientation upon exposure of the organism to blue light. Focusing on the question how the new orientation of the CA is long time maintained by the cell, we identified in a small difference in the dynamics of differently oriented microtubules a plausible factor that causes the maintained reorientation of the CA. Intriguingly, our findings have the potential to be applied to different systems at different size-scales. Indeed, our proposed mechanism is a fascinating example of competitive exclusion principle in population ecology [18]. According to that principle, two populations competing for the same limited resources cannot coexist at equilibrium. Instead, the competitively superior population will persist while the other will go extinct. In this light, our predicted persistence of few microtubules polarized in the transverse direction is caused by three regulating factors that prevent the extinction of the initial transverse array: the occasional occurrence of severing events for transverse microtubules, the few dispersed nucleation events in the transverse direction, and the microtubule-based nucleation of transverse from longitudinal microtubules. When none of those three factors is present, as in the $\lambda_* \to 0$ case of Section III B, only the longitudinal array would persist.

Our study of the reorientation of the cortical microtubule array raised some questions and problems. Firstly, an experimental observation of a difference in any of the dynamic parameters between differently oriented microtubules is, at present, lacking. Nevertheless, our theoretical predictions can be, in principle, experimentally tested by performing extensive data analysis on the dynamic parameters of cortical microtubules of *Arabidopsis thaliana* during the reorientation of the cortical array. According to our model, the detection of a very small difference between the dynamics of longitudinal and transverse microtubules would be a sufficient proof to experimentally confirm our theoretical predictions. Should the difference in the dynamics for differently oriented microtubules be confirmed, the following research step would be understanding the underlying mechanism behind such a difference. A possible cause could be the different mechanical stress undergone by microtubules as a consequence of cell wall geometry. Indeed, while longitudinal microtubules grow on a roughly flat surface, transverse microtubules undergo dynamic instability on a curved surface. Previous experimental and computational works have in fact revealed that a single preferential direction of ordering of the CA can be influenced - among other factor, by geometry-induced mechanical stress, or catastrophe induced at sharp cell edges [8, 11, 12].

Besides the search for an experimental confirmation of our hypothesis on the underlying mechanism behind a maintained reorientation, our investigation also lacks a full, comprehensive computational verification. Indeed, although our model can explain the long time maintenance of the reoriented array, it is still too idealized to completely represent

the dynamics of cortical microtubules in the cell. More precisely, in our model microtubules live in two non-physical spaces, with the possibility to interact only through the overall properties of the entire population they belong to. Thus, a computational approach that takes into account the geometry of the cell, the creation of crossovers, and the dynamics induced by the interaction between different microtubules, like, e.g., severing events, induced catastrophes, or zippering, could be used to further prove (or disprove) our theoretical predictions. On the one hand, taking all this factors into consideration would create a high degree of complexity for the model, impeding a full, analytical description. On the other hand, there exists a computational framework that has the potential to properly address the problem [11, 19]. This framework consists of a set of triangular approximations of arbitrary areas of the cell surface, where microtubules undergo dynamic instability and can interact with each other for crossover creation events, as well as severing or zippering. This computational framework can already predict the reaching of an ordered state for microtubules that align while starting from an isotropic condition [20]. The addition of a bias in the speed of growing microtubules depending on their growing direction would, in principle, computationally test in a more realistic scenario whether or not the speed difference can explain a reorientation of the array and its maintenance.

At first sight, our result that preferential severing for longitudinal microtubules and high probability of stabilization-after-severing are not necessary for the maintenance of the longitudinal array, seems in contrast with previous experiments and theory [6, 7], where those two factors have been identified as crucial for the start of the reorientation. However, our computational results revealed that preferential severing and high probability of stabilization-after-severing play a key role in quickly initiating the reorientation, in agreement with the results of the previous works.

V. ACKNOWLEDGEMENT

The work of M.S. was supported by the ERC 2013 Synergy Grant MODELCELL. The work of B.M.M. is part of the research program of the Dutch Research Council (NWO). We thank Jelmer Lindeboom for a careful reading of the manuscript and for providing Figure 1A.

VI. SUPPLEMENTARY INFORMATION

A. Steady-state solution for the microtubule length distribution

Dynamic equations

Let $m^{\tau}(t,l)$ be the probability distribution of the length of microtubules in the state τ at time t. Following Tindemans and Mulder [21], it is possible to show that the dynamic equations that govern the model are

$$\begin{aligned}\frac{\partial}{\partial t}m_{\parallel}^{+}(t,l) = &-\alpha V^{+}(L_f)\frac{\partial}{\partial l}m_{\parallel}^{+}(t,l) - r_c m_{\parallel}^{+}(t,l) + r_r m_{\parallel}^{-}(t,l)\\ &- q\, r_s\, l\, L_{\perp}\, m_{\parallel}^{+}(t,l) + q\, r_s\left(1+p^{+}\right)L_{\perp}\left[M_{\parallel}^{+}(t,l) + M_{\parallel}^{-}(t,l)\right]\\ &+ q\, r_s L_{\perp} M_{\parallel}^{+}(t,l)\,,\end{aligned} \tag{37}$$

$$\begin{aligned}\frac{\partial}{\partial t}m_{\parallel}^{-}(t,l) = &\; v^{-}\frac{\partial}{\partial l}m_{\parallel}^{-}(t,l) - r_r m_{\parallel}^{-}(t,l) + r_c m_{\parallel}^{+}(t,l)\\ &- q\, r_s\, l\, L_{\perp}\, m_{\parallel}^{-}(t,l) + q\, r_s\left(1-p^{+}\right)L_{\perp}\left[M_{\parallel}^{+}(t,l) + M_{\parallel}^{-}(t,l)\right]\\ &+ q\, r_s L_{\perp} M_{\parallel}^{-}(t,l)\,,\end{aligned} \tag{38}$$

$$\begin{aligned}\frac{\partial}{\partial t}m_{\perp}^{+}(t,l) = &-V^{+}(L_f)\frac{\partial}{\partial l}m_{\perp}^{+}(t,l) - r_c m_{\perp}^{+}(t,l) + r_r m_{\perp}^{-}(t,l)\\ &- (1-q)\, r_s\, l\, L_{\parallel}\, m_{\perp}^{+}(t,l)\\ &+ (1-q)\, r_s\left(1+p^{+}\right)L_{\parallel}\left[M_{\perp}^{+}(t,l) + M_{\perp}^{-}(t,l)\right]\\ &+ (1-q)\, r_s L_{\parallel} M_{\perp}^{+}(t,l)\,,\end{aligned} \tag{39}$$

$$\begin{aligned}\frac{\partial}{\partial t}m_{\perp}^{-}(t,l) = v^{-}\frac{\partial}{\partial l}m_{\perp}^{-}(t,l) - r_r m_{\perp}^{-}(t,l) + r_c m_{\perp}^{+}(t,l)\\ -(1-q)\,r_s\,l\,L_{\parallel}\,m_{\perp}^{-}(t,l)\\ +(1-q)\,r_s\left(1-p^{+}\right)L_{\parallel}\left[M_{\perp}^{+}(t,l)+M_{\perp}^{-}(t,l)\right]\\ +(1-q)\,r_s L_{\parallel} M_{\perp}^{-}(t,l)\,,\end{aligned} \tag{40}$$

with boundary conditions

$$\alpha V^{+}(L_f)\,m_{\parallel}^{+}(t,0) = R_n^{\parallel}\left(L_f, L_{\parallel}\right), \tag{41}$$

$$V^{+}(L_f)\,m_{\perp}^{+}(t,0) = R_n^{\perp}\left(L_f, L_{\perp}\right), \tag{42}$$

$$\lim_{l\to\infty} m_{\parallel/\perp}^{-}(t,l) = 0, \tag{43}$$

and initial conditions from the steady-state solution of the Dogterom-Leibler model, i.e.,

$$m_{\parallel}^{+}(0,l) = 0, \tag{44}$$

$$m_{\parallel}^{-}(0,l) = 0, \tag{45}$$

$$m_{\perp}^{+}(0,l) = \frac{R_n(L_f)}{V^{+}(L_f)}\,\exp\left[-\left(\frac{r_c}{V^{+}(L_f)}-\frac{r_r}{v^{-}}\right)l\right], \tag{46}$$

$$m_{\perp}^{-}(0,l) = \frac{R_n(L_f)}{v^{-}}\,\exp\left[-\left(\frac{r_c}{V^{+}(L_f)}-\frac{r_r}{v^{-}}\right)l\right]. \tag{47}$$

It is convenient to underline that the total amount of tubulin polarized in either of the two directions is linked to the microtubule length distributions through the equations

$$L_{\parallel}(t) = \int_0^{\infty} dl\,l\left[m_{\parallel}^{+}(t,l)+m_{\parallel}^{-}(t,l)\right], \tag{48}$$

$$L_{\perp}(t) = \int_0^{\infty} dl\,l\left[m_{\perp}^{+}(t,l)+m_{\perp}^{-}(t,l)\right], \tag{49}$$

i.e., the total amount of tubulin used by longitudinal/transverse microtubules is the first moment of the total length distribution of longitudinal/transverse microtubules.

Steady-state solution

The dependency of the growing speed of microtubules on the amount of free tubulin L_f in the pool implies that the microtubule length distribution eventually reaches the steady-state. Here, in order to find an analytical solution, we make the further assumption that microtubules undergo complete depolymerization suddenly after a catastrophe, i.e.,

$$\frac{\langle l\rangle}{v^{-}} \ll \frac{1}{r_r}, \tag{50}$$

where $\langle l\rangle$ is the mean length of a microtubule in the system. In this limit we can identify all microtubules with the growing microtubules and, therefore, to ease the notation we remove the label + from all microtubule distributions. Thus, Eqs. (37-40) are replaced by

$$0 = -\alpha V^{+}\frac{d}{dl}m_{\parallel}(l) - r_c m_{\parallel}(l) - q\,r_s\,l\,L_{\perp}\,m_{\parallel}(l) + q\,r_s\left(1+p^{+}\right)L_{\perp}M_{\parallel}(l)\,, \tag{51}$$

$$0 = -V^{+}\frac{d}{dl}m_{\perp}(l) - r_c m_{\perp}(l) - (1-q)\, r_s\, l\, L_{\parallel}\, m_{\perp}(l) + (1-q)\, r_s \left(1+p^{+}\right) L_{\parallel} M_{\perp}(l)\,. \tag{52}$$

If we differentiate by l the last two equations we obtain

$$\alpha V^{+}\frac{d^2}{dl^2}m_{\parallel}(l) + (r_c + q\, r_s L_{\perp}\, l)\frac{d}{dl}m_{\parallel}(l) + q\, r_s L_{\perp}\left(2+p^{+}\right) m_{\parallel}(l) = 0, \tag{53}$$

$$V^{+}\frac{d^2}{dl^2}m_{\perp}(l) + \left(r_c + (1-q)\, r_s L_{\parallel}\, l\right)\frac{d}{dl}m_{\perp}(l) + (1-q)\, r_s L_{\parallel}\left(2+p^{+}\right) m_{\perp}(l) = 0. \tag{54}$$

As $L_{\parallel/\perp} = \int_0^{\infty} dl\, m_{\parallel/\perp}(l)$, Eqs. (53) and (54) are coupled second order differential equations, and they are also linked to Eq. (1) through $V^{+}(L_f)$. However, L_f, $L_{\parallel}$, and $L_{\perp}$ do not depend on l, hence Eqs. (53) and (54) can be in principle solved, with solutions that depend on the total amount of tubulin used by the other population and on the free tubulin. We re-write the two equations in a more elegant way as

$$\frac{d^2}{d\lambda^2}\mu_{\parallel}(\lambda) + (1 + q\,\sigma\Lambda_{\perp}\,\lambda)\frac{d}{d\lambda}\mu_{\parallel}(\lambda) + q\,\sigma\Lambda_{\perp}\left(2+p^{+}\right)\mu_{\parallel}(\lambda) = 0, \tag{55}$$

$$\frac{d^2}{d\lambda^2}\mu_{\perp}(\lambda) + \left(1 + (1-q)\,\sigma\Lambda_{\parallel}\,\lambda\right)\frac{d}{d\lambda}\mu_{\perp}(\lambda) + (1-q)\,\sigma\Lambda_{\parallel}\left(2+p^{+}\right)\mu_{\perp}(\lambda) = 0, \tag{56}$$

where we introduce the non-dimensional quantities

$$\lambda = \frac{r_c}{V^{+}} l, \tag{57}$$

$$\Lambda_{\parallel/\perp} = \frac{r_c}{V^{+}} L_{\parallel/\perp}, \tag{58}$$

$$\mu_{\parallel/\perp} = \frac{V^{+}}{R_n^{\parallel/\perp}} m_{\parallel/\perp}, \tag{59}$$

$$\sigma = \frac{r_s \left(V^{+}\right)^2}{r_c^3}, \tag{60}$$

and we incorporate the factor α in the parameter V^{+} for longitudinal microtubules. Notice that, with this non-dimensionalization, all parameters of the model - including the independent variable λ, are functions of L_f as they depend on $V^{+}(L_f)$.

To solve Eq. (55), we first notice that the asymptotic solution for large λ decays as $\exp\left(-\frac{1}{2}q\sigma\Lambda_{\perp}\lambda^2 - \lambda\right)$. Therefore, we suppose there exists a function $\xi_{\parallel}(\lambda)$ such that

$$\mu_{\parallel}(\lambda) = \exp\left(-\frac{1}{2}q\sigma\Lambda_{\perp}\lambda^2 - \lambda\right)\xi_{\parallel}(\lambda)\,. \tag{61}$$

If we plug this in Eq. (55) we obtain

$$\frac{d^2}{d\lambda^2}\xi_{\parallel}(\lambda) - (1 + q\,\sigma\Lambda_{\perp}\,\lambda)\frac{d}{d\lambda}\xi_{\parallel}(\lambda) + q\,\sigma\Lambda_{\perp}\left(1+p^{+}\right)\xi_{\parallel}(\lambda)\,. \tag{62}$$

If we change variable as $x = (1 + q\,\sigma\Lambda_{\perp}\lambda)/\sqrt{2q\,\sigma\Lambda_{\perp}}$, last equation becomes

$$\frac{d^2}{dx^2}\xi_{\parallel}(x) - 2x\frac{d}{dx}\xi_{\parallel}(x) + 2\left(1+p^{+}\right)\xi_{\parallel}(x)\,, \tag{63}$$

i.e., the Hermite equation [22], the solution of which is the Hermite function

$$\xi_{\parallel}(x) = H_{1+p^{+}}(x)\,. \tag{64}$$

Therefore, the full solution for $\mu_{\parallel}$ becomes

$$\mu_{\parallel}(\lambda) = \frac{H_{1+p^+}\left((1+q\,\sigma\Lambda_{\perp}\lambda)/\sqrt{2q\,\sigma\Lambda_{\perp}}\right)}{H_{1+p^+}\left(1/\sqrt{2q\,\sigma\Lambda_{\perp}}\right)}\,\exp\left[-\frac{1}{2}q\sigma\Lambda_{\perp}\lambda^2-\lambda\right], \tag{65}$$

and, similarly,

$$\mu_{\perp}(\lambda) = \frac{H_{1+p^+}\left(\left(1+(1-q)\,\sigma\Lambda_{\parallel}\lambda\right)/\sqrt{2\,(1-q)\,\sigma\Lambda_{\parallel}}\right)}{H_{1+p^+}\left(1/\sqrt{2\,(1-q)\,\sigma\Lambda_{\parallel}}\right)}\,\exp\left[-\frac{1}{2}\,(1-q)\,\sigma\Lambda_{\parallel}\lambda^2-\lambda\right]. \tag{66}$$

Eqs. (65) and (66) highlight a peculiar property of the model. Indeed, if $p^+ \neq 0$, both denominators of the two distribution can be identically 0. In other words, there exist two values of σ such that $H_{1+p^+}\left(1/\sqrt{2q\,\sigma\Lambda_{\perp}}\right)=0$ or $H_{1+p^+}\left(1/\sqrt{2\,(1-q)\,\sigma\Lambda_{\parallel}}\right)=0$, with the consequence that the number of longitudinal/transverse microtubules diverges. In the analytically tractable $p^+=1$ case these values are $\sigma=\frac{1}{q\Lambda_{\perp}}$ for the divergence of the longitudinal, and $\sigma=\frac{1}{(1-q)\Lambda_{\parallel}}$ for the divergence of the transverse microtubules.

B. The initial transverse array

To keep with the assumption coming from the experiments that initially all cortical microtubules are directed transversely to the growth direction of the cell, we build the initial array by considering dispersed and microtubule-based nucleation possible only in the transverse direction. In other words, for the creation of the initial array, we impose

$$R_n^{\parallel}=0,$$

$$R_n^{\perp}=r_n\frac{L_f^a}{L_f^a+L_v^a}=R_n\left(L_f\right).$$

Therefore, the dynamics of the initial array is fully described by the Dogterom-Leibler model. Furthermore, the dependency of the growing speed of microtubules on the amount of free tubulin L_f in the pool implies that the microtubule length distribution eventually reaches the steady-state even in the case of initially unbounded-growth microtubules (Tindemans et al., Front. Phys., 2014). Thus, the solution of the model is the steady-state solution of Dogterom-Leibler model. Such a solution for the distribution of the length of microtubules is the initial condition for our model, see Supplementary Information VI A.

C. Polarization and suppression in case of no difference in the growing speed of different populations

Here, we show that the sole asymmetry in the system consequent to the preferential severing cannot explain the full, maintained reorientation observed in the experiments. Similarly as in Result section, we perform a sensitivity analysis by separately tuning q and p^+ from 0 to 1, and we measure number and length polarization and suppression, and the time needed by the system to achieve the reorientation, averaged over $N=10^3$ simulations. Parameters and relative numerical values used in the simulations are listed in Table I. However, since we are considering the case in which differently oriented microtubules have the same growing speed, in this case $\alpha=1$.

Figure 5ABE shows that the system does not exhibit longitudinal polarization at the equilibrium for biologically realistic p^+, i.e., for p^+ comprises between 0 and 0.25. Similarly, Figure 5CD shows that in the same range of values, although we can appreciate some degree of transverse suppression, the initial transverse array does not disappear. On the other hand, Figure 5 reveals the existence of two regions in the (q,p^+) plane where the reorientation occurs and it is fast, namely, when both q and p^+ are high and, surprisingly, when they are both low. While one can easily argue that a high value of both q and p^+ is associated to a greater likelihood of increasing the size of the longitudinal population and the lifetime of their individuals and, hence, the longitudinal polarization, it is more difficult to intuitively understand the behaviour of the system for low values of those probabilities. However, lower values of q and p^+ are linked to an effective shortening of the single transverse microtubules and, therefore, to a fall in their average lifetime. As a consequence, the overall length used by the transverse array shortens, and so does the number of transverse microtubules, as their nucleation is partly correlated to the length polarized in the transverse direction. Nevertheless, although narrow areas in the heat maps of Figure 5 where a full and maintained reorientation of the CA

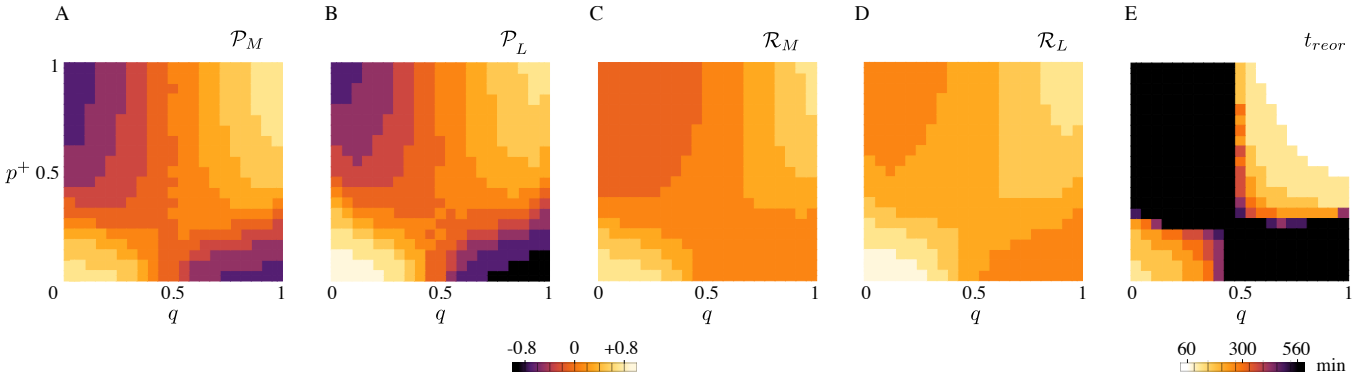

Figure 5. (A) Microtubule number polarization, (B) microtubule length polarization, (C) transverse number suppression, (D) transverse length suppression, (E) and transverse-to-longitudinal reorientation time as functions of q and p^+. Lighter colors correspond to a more efficient reorientation. (A, B, C, D) The range of values for polarization and suppression runs from -1 to $+1$. (E) Black areas in the (q, p^+) plane correspond both to reorientation processes that required more than 540 minutes, or non-occurred reorientation. Results are averaged over $N = 10^3$ simulations.

occurs do exist, a comparison with the Figure 2 would immediately show that in the latter case the same areas are wider.

As the only asymmetry between the two populations of the system is due to the probability q, Figure 5AB displays, as expected, the symmetry $\mathcal{P} \to -\mathcal{P}$, as $q \to 1 - q$ for both $\mathcal{P}_M$ and $\mathcal{P}_L$.

Although from these results one can conclude that the preferential severing for the longitudinal microtubules cannot explain the maintenance of the array in the longitudinal direction, at least in the biological range of values for p^+, the dynamic behaviour of the two microtubule populations for high values of q and p^+ highlights an interesting fact. Indeed, Figure 5E shows that high values of p^+ and q are associated with fast reorientation, showing that, even though the preferential severing for longitudinal microtubules and a high probability of stabilization-after-severing are neither necessary nor sufficient to achieve CA reorientation, they are able to accelerate this process significantly.

The amount of free tubulin in the pool does not substantially change from the initial value where only transverse microtubules are present, to the final steady-state value, see Figure 6B. This means that all the building material used by the longitudinal microtubules to create the new array comes from the suppression of the initial transverse array. Curiously, Figure 6A also shows that at the start of the reorientation process, i.e., at $t = 0$, there is a sudden little drop of the number of transverse microtubules. This may be explained by the sudden change in the nucleation rate of old microtubules, as it switches from R_n to $R_n/2$ as a consequence of the imposed isotropy of the system.

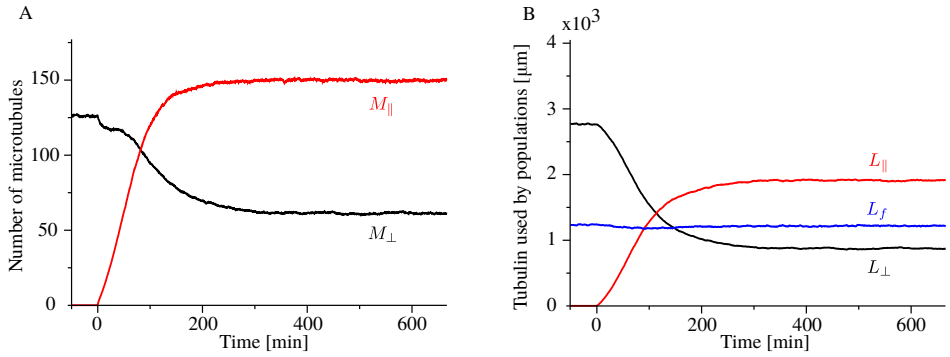

Figure 6. Time evolution of (A) longitudinal (red) and transverse (black) microtubules, and (B) tubulin used by the longitudinal population (red), the transverse population (black), and the free tubulin (blue), averaged over $N = 10^3$ simulations. Here, we used $q = 0.8$ and $p^+ = 0.6$.

D. Time-dependent solution of the non-interacting model

We look for an expression for the time scale of the reorientation of the array from the transverse to the longitudinal direction to the growth direction of the cell. We focus on Eqs. (17) and (19), with their respective boundary conditions

$$M_{\parallel}(0) = 0 = L_{\parallel}(0).$$

By plugging these boundary conditions in Eqs. (17) and (19) we obtain the boundary conditions for the first derivative of both $M_{\parallel}$ and $L_{\parallel}$

$$\left.\frac{dM_{\parallel}(t)}{dt}\right|_{t=0} = R_n \frac{\frac{1}{2}L_*}{L_{tot} - L_f + L_*},$$

$$\left.\frac{dL_{\parallel}(t)}{dt}\right|_{t=0} = 0.$$

Eqs. (17) and (19) can be decoupled to obtain

$$\frac{d^2 L_{\parallel}(t)}{dt^2} + 2r_c \frac{dL_{\parallel}(t)}{dt} + \left(r_c^2 - \alpha V^+ \widetilde{R}_n\right) L_{\parallel}(t) = \alpha V^+ \widetilde{R}_n \frac{1}{2} L_*, \tag{67}$$

and

$$\frac{d^2 M_{\parallel}(t)}{dt^2} + 2r_c \frac{dM_{\parallel}(t)}{dt} + \left(r_c^2 - \alpha V^+ \widetilde{R}_n\right) M_{\parallel}(t) = r_c \widetilde{R}_n \frac{1}{2} L_*, \tag{68}$$

where we defined

$$\widetilde{R}_n = \frac{R_n}{L_{tot} - L_f + L_*}.$$

Eqs. (67) are second order non-homogeneous differential equations, the solutions of which are

$$\begin{aligned} L_{\parallel}(t) = {} & \frac{1}{2} L_* \frac{\alpha V^+ \widetilde{R}_n}{r_c^2 - \alpha V^+ \widetilde{R}_n} + \frac{1}{2} L_* \frac{\sqrt{\alpha V^+ \widetilde{R}_n}}{2\left(r_c^2 - \alpha V^+ \widetilde{R}_n\right)} \\ & \times \left[\left(r_c - \sqrt{\alpha V^+ \widetilde{R}_n}\right) e^{-\left(r_c + \sqrt{\alpha V^+ \widetilde{R}_n}\right)t} - \left(r_c + \sqrt{\alpha V^+ \widetilde{R}_n}\right) e^{-\left(r_c - \sqrt{\alpha V^+ \widetilde{R}_n}\right)t}\right], \end{aligned} \tag{69}$$

$$\begin{aligned} M_{\parallel}(t) = {} & \frac{1}{2} L_* \frac{r_c \widetilde{R}_n}{r_c^2 - \alpha V^+ \widetilde{R}_n} + \frac{1}{2} L_* \frac{\widetilde{R}_n}{2\left(r_c^2 - \alpha V^+ \widetilde{R}_n\right)} \\ & \times \left[\left(\sqrt{\alpha V^+ \widetilde{R}_n} + r_c\right) e^{-\left(r_c - \sqrt{\alpha V^+ \widetilde{R}_n}\right)t} - \left(\sqrt{\alpha V^+ \widetilde{R}_n} - r_c\right) e^{-\left(r_c + \sqrt{\alpha V^+ \widetilde{R}_n}\right)t}\right]. \end{aligned} \tag{70}$$

These expressions define the time scale of the reorientation process, i.e.

$$t_{reor} \propto \left(r_c - \sqrt{\alpha V^+ \widetilde{R}_n}\right)^{-1}. \tag{71}$$

To highlight all dependencies of t_{reor} on the model parameters, we can conveniently rewrite $\alpha V^+ \widetilde{R}_n$ by expressing all quantities as functions of L_f. We find

$$\alpha V^+ \widetilde{R}_n = \alpha v^+ r_n \frac{L_f}{L_f + L_v} \frac{L_f^a}{L_f^a + L_v^a} \frac{1}{L_{tot} - L_f + L_*} = r_c^2 \frac{\alpha}{\alpha + \frac{1}{2}\frac{L_*}{L_{tot} - L_f}(\alpha + 1)}.$$

Thus, the time scale of the reorientation can be written now as

$$t_{reor} \propto \left[r_c \left(1 - \sqrt{\frac{\alpha \left(L_{tot} - L_f \right)}{\alpha \left(L_{tot} - L_f \right) + \frac{1}{2} L_* \left(\alpha + 1 \right)}} \right) \right]^{-1}. \tag{72}$$

L_f is weakly dependent on r_c. As a consequence, Eq. (72) reveals that the time scale of the reorientation is inversely proportional to the catastrophe rate. The interpretation of this counter-intuitive result, is that every time a microtubule undergoes a catastrophe, it releases to the free tubulin pool an amount of tubulin equal to its length. Therefore, the amount of building material available for the new array increases with higher rate, and so does the speed of reorientation.

E. Polarization and transverse suppression in the non-interacting model

We calculate the reorientation polarization and transverse suppression. From Eqs. (30-33) we obtain

$$\mathcal{P}_M = \frac{M_\parallel - M_\perp}{M_\parallel + M_\perp} = \frac{\left(\alpha - 1 \right) \left(1 - \frac{1}{2} \lambda_* \right)}{\left(1 + \lambda_* \right) \left[\left(\alpha - 1 \right) + \frac{1}{2} \lambda_* \left(\alpha + 1 \right) \right]}, \tag{73}$$

and

$$\mathcal{P}_L = \frac{L_\parallel - L_\perp}{L_\parallel + L_\perp} = \frac{\left(\alpha - 1 \right) \left(1 + \frac{1}{2} \lambda_* \right)}{\left(\alpha - 1 \right) + \frac{1}{2} \lambda_* \left(\alpha + 1 \right)}. \tag{74}$$

As expected, both reorientation parameters are close to 1 when λ_* is small, see Figure 7AB, whilst they rapidly decay to 0 for higher values of λ_*.

Similarly, we can calculate the transverse suppression:

$$\mathcal{R}_M = \frac{M_\perp^0 - M_\perp}{M_\perp^0 + M_\perp} = \frac{\left(\frac{1}{2} \lambda_* \right)^2 \left(\alpha + 1 \right) + \frac{1}{2} \lambda_* \left(2\alpha - 1 \right) + \left(\alpha - 1 \right)}{3 \left(\frac{1}{2} \lambda_* \right)^2 \left(\alpha + 1 \right) + \frac{1}{2} \lambda_* \left(4\alpha - 1 \right) + \left(\alpha - 1 \right)}, \tag{75}$$

and

$$\mathcal{R}_L = \frac{L_\perp^0 - L_\perp}{L_\perp^0 + L_\perp} = \frac{\alpha \left(1 + \frac{1}{2} \lambda_* \right) - 1}{\alpha \left(1 + \frac{1}{2} \lambda_* \right) - 1 + \lambda_*}. \tag{76}$$

Figure 7CD shows that in the case of the transverse suppression the effect of the bias in the speed is to almost completely remove the initial transverse array.

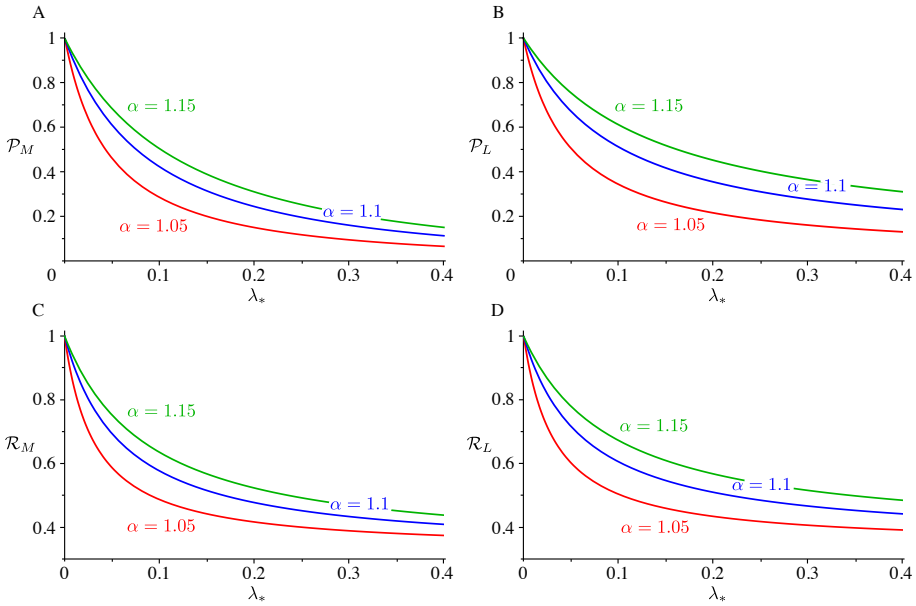

Figure 7. Polarization for (A) the microtubules and (B) the tubulin, and suppression for (C) microtubules number and (D) length as a function of the propensity length for dispersed nucleation for $\alpha = 1.05$ (red), $\alpha = 1.1$ (blue), and $\alpha = 1.15$ (green).

[1] Ram Dixit and Richard Cyr. The cortical microtubule array: From dynamics to organization, oct 2004.

[2] Takashi Murata, Seiji Sonobe, Tobias I. Baskin, Susumu Hyodo, Seiichiro Hasezawa, Toshiyuki Nagata, Tetsuya Horio, and Mitsuyasu Hasebe. Microtubule-dependent microtubule nucleation based on recruitment of γ-tubulin in higher plants. *Nat. Cell Biol.*, 7(10):961–968, oct 2005.

[3] Jordi Chan, Adrian Sambade, Grant Calder, and Clive Lloyd. Arabidopsis cortical microtubules are initiated along, as well as branching from, existing microtubules. *Plant Cell*, 21(8):2298–2306, aug 2009.

[4] Jelmer J. Lindeboom, Masayoshi Nakamura, Anneke Hibbel, Kostya Shundyak, Ryan Gutierrez, Tijs Ketelaar, Anne Mie C. Emons, Bela M. Mulder, Viktor Kirik, and David W. Ehrhardt. A mechanism for reorientation of cortical microtubule arrays driven by microtubule severing. *Science (80-.).*, 342(6163), dec 2013.

[5] Masayoshi Nakamura, Jelmer J. Lindeboom, Marco Saltini, Bela M. Mulder, and David W. Ehrhardt. SPR2 protects minus ends to promote severing and reorientation of plant cortical microtubule arrays. *J. Cell Biol.*, 217(3):915–927, mar 2018.

[6] Jelmer J. Lindeboom, Masayoshi Nakamura, Marco Saltini, Anneke Hibbel, Ankit Walia, Tijs Ketelaar, Anne Mie C. Emons, John C. Sedbrook, Viktor Kirik, Bela M. Mulder, and David W. Ehrhardt. CLASP stabilization of plus ends created by severing promotes microtubule creation and reorientation. *J. Cell Biol.*, 218(1):190–205, jan 2019.

[7] Marco Saltini and Bela M. Mulder. Critical threshold for microtubule amplification through templated severing. *Phys. Rev. E*, 101(5):052405, may 2020.

[8] Olivier Hamant, Marcus G. Heisler, Henrik Jönsson, Pawel Krupinski, Magalie Uyttewaal, Plamen Bokov, Francis Corson, Patrik Sahlin, Arezki Boudaoud, Elliot M. Meyerowitz, Yves Couder, and Jan Traas. Developmental patterning by mechanical signals in arabidopsis. *Science*, 322(5908):1650–1655, 2008.

[9] Benoît Landrein and Olivier Hamant. How mechanical stress controls microtubule behavior and morphogenesis in plants: history, experiments and revisited theories. *Plant J.*, 75(2):324–338, jul 2013.

[10] Magalie Uyttewaal, Agata Burian, Karen Alim, Benoît Landrein, Dorota Borowska-Wykręt, Annick Dedieu, Alexis Peaucelle, Michał Ludynia, Jan Traas, Arezki Boudaoud, Dorota Kwiatkowska, and Olivier Hamant. Mechanical stress acts via katanin to amplify differences in growth rate between adjacent cells in arabidopsis. *Cell*, 149(2):439 – 451, 2012.

[11] Bandan Chakrabortty, Ikram Blilou, Ben Scheres, and Bela M. Mulder. A computational framework for cortical microtubule dynamics in realistically shaped plant cells. *PLoS Comput. Biol.*, 14(2):e1005959, feb 2018.

[12] Vincent Mirabet, Pawel Krupinski, Olivier Hamant, Elliot M. Meyerowitz, Henrik Jönsson, and Arezki Boudaoud. The self-organization of plant microtubules inside the cell volume yields their cortical localization, stable alignment, and sensitivity to external cues. *PLOS Computational Biology*, 14(2):1–23, 02 2018.

[13] Marileen Dogterom and Stanislas Leibler. Physical aspects of the growth and regulation of microtubule structures. *Phys. Rev. Lett.*, 70(9):1347–1350, mar 1993.

[14] Michal Wieczorek, Susanne Bechstedt, Sami Chaaban, and Gary J. Brouhard. Microtubule-associated proteins control the kinetics of microtubule nucleation. *Nat. Cell Biol.*, 17(7):907–916, jul 2015.

[15] David W. Ehrhardt. Straighten up and fly right-microtubule dynamics and organization of non-centrosomal arrays in higher

plants, feb 2008.

[16] Eva E. Deinum, Simon H. Tindemans, and Bela M. Mulder. Taking directions: The role of microtubule-bound nucleation in the self-organization of the plant cortical array. *Phys. Biol.*, 8(5), oct 2011.

[17] Eva E. Deinum, Simon H. Tindemans, Jelmer J. Lindeboom, and Bela M. Mulder. How selective severing by katanin promotes order in the plant cortical microtubule array. *Proc. Natl. Acad. Sci. U. S. A.*, 114(27):6942–6947, jul 2017.

[18] Garrett Hardin. The competitive exclusion principle. *Science (80-.).*, 131(3409):1292–1297, apr 1960.

[19] Simon H. Tindemans, Eva E. Deinum, Jelmer J. Lindeboom, and Bela M. Mulder. Efficient event-driven simulations shed new light on microtubule organization in the plant cortical array. *Front. Phys.*, 2:1–15, apr 2014.

[20] Simon H. Tindemans, Rhoda J. Hawkins, and Bela M. Mulder. Survival of the aligned: Ordering of the plant cortical microtubule array. *Phys. Rev. Lett.*, 104(5):058103, feb 2010.

[21] Simon H. Tindemans and Bela M. Mulder. Microtubule length distributions in the presence of protein-induced severing. *Phys. Rev. E - Stat. Nonlinear, Soft Matter Phys.*, 81(3):031910, mar 2010.

[22] Richard Courant and David Hilbert. *Methods of Mathematical Physics*. Wiley-Interscience, 1989.